PCCP

Accepted Manuscript

This article can be cited before page numbers have been issued, to do this please use: Z. Haider, J. Y. Zheng and Y. S. Kang, *Phys. Chem. Chem. Phys.*, 2016, DOI: 10.1039/C6CP01740A.

ROYAL SOCIETY OF CHEMISTRY

www.rsc.org/pccp

View Article Online
DOI: 10.1039/C6CP01740A

Journal Name

ARTICLE

Surfactant Free Fabrication and Improved Charge Carrier Separation Induced Enhanced Photocatalytic Activity of {001} Facet Exposed Unique Octagonal BiOCl Nanosheets

Received 00th January 20xx,
Accepted 00th January 20xx

DOI: 10.1039/x0xx00000x

www.rsc.org/

Zeeshan Haider, Jin You Zheng and Young Soo Kang*

Unique octagonal shaped BiOCl nanosheets (NS) dominantly exposed with high energy, {001} crystal facet have been fabricated via simple hydrothermal route without using organic surfactants. Dynamics of photogenerated charge carriers have been studied by time resolved photoluminescence spectroscopy. Fitting parameters of decay kinentcs were used to calculate both intensity weighted average lifetime ($\langle\tau\rangle_{int.}$) as well as amplitude weighted average lifetime ($\langle\tau\rangle_{amp.}$) of photogenerated charge carreirs. $\langle\tau\rangle_{int.}$ and $\tau\rangle_{amp.}$ of {001} BiOCl NS, i.e 17.23 ns and 1.94 ns was observed significantly higher than corresponding values of pristine BiOCl such as 2.52 ns and 1.07 ns. Significant quenching in PL emission intensity of {001} BiOCl NS reflected enhanced seperation of photogenerated charge carriers. Reduced thickness and in-situ iodine doping was favorable to minimize recombination tendency. Photocatalytic activity was monitored by photodegradation of RhB under visible light illumination (λ > 400 nm). {001} BiOCl NS exhibited superior performance than pristine BiOCl in term of rapid degradation kinetics and higher photonic efficiency. Photocatalytic efficiency of {001} BiOCl NS was 2.8 times higher than pristine BiOCl. Iodine doping induced extended optical absorption in the visible region and improved seperation of photogenerated charge carreirs played an important role to enhance photocatalytic activity. Photodegradation mechanism was systematically studied by using various radical quenchers and it was revealed that photogenerated holes (h^+) and superoxide radicals ($^{\cdot}O^{2-}$) actively participated whereas hydroxyl (OH^-) radicals had negligible contribution in photodegradation of RhB. {001} BiOCl NS has shown higher photocurrent density and lower charge transfer resistance analyzed through photoelectrochemical and electrochemical impedance measurements. This work highlights fabrication of unique octagonal BiOCl NS with improved seperation of charge carriers across high energy crystal facts to design highly efficient photocatalyst.

Introduction

Crystal facet engineering has attained enormous attention for improvement in performance of photocatalytic materials. It has derived reshaping of nanocrystals into versatile morphologies. Such efforts can be useful to develop novel materials suitable for commercial applications. Both experimental and theoretical findings have suggested correlation of photocatalytic activity with exposed crystal facets.[1] Designing of semiconductors such as TiO_2[1], ZnO[2], Fe_2O_3,[3] Cu_2O,[4] WO_3,[5] and $BiVO_4$[6] with exposed crystal facets have gained specialized attention. Our group has also reported crystal facet engineering of various oxide semiconductors.[7-11] The difference in performance of various crystal facets is linked with unique surface features, such as local electronic structure,[12] atomic termination,[13] atomic population,[14] co-ordination patterns,[1] dangling bonds,[15] internal electric strain[16] as well as surface energies.[17] In general high energy facets are more reactive compared to lower energy counterparts[18], however during hydrothermal growth formation of low energy facets is more favourale.[1] Controlled fabrication of high energy facets usually involve the use of various organic surfactants as a structure directing agents.[19] One of the potential draw backs associated with use of organic surfactants is that they can hamper interfacial charge transfer phenomena.[20] On the other hand surfactant free synthesis of high energy facets with controlled morphologies has been quite challenging.

Bismuth oxychloride (BiOCl) has tetragonal structures (lattice parameters, a = b = 0.389 nm, c = 0.789 nm.[26] It has been synthesized in variety of shapes such as nanosheets,[16] hierarchical spheres[21] and nanofibers[22] by different routes such as vapour phase,[23] electrochemical,[24] micro-emulsion[25]

[a] Korea Center for Artificial Photosynthesis and Department of Chemistry,
[b] Sogang University, Seoul 121-742, Republic of Korea
[c] Email: yskang@sogang.ac.kr

†**Electronic Supplementary Information (ESI) available:** [Elemental mapping, EDX spectra of {001} BiOCl NS, crystal model and c-axis projection of BiOCl, percentage calculation of exposed {001} facet, SEM images of {001} BiOCl NS prepared under variable solvent ratio, XRD patterns and SEM images with various precursors of $Bi3^+$ and I^-, wavelength dependent output irradiation of 300 W Xenon lamp fitted with 400 nm long pass filter, absorption spectra of RhB, plot of lnC/C_o versus irradiation time, rate constant for photodegradation of RhB normalized to BET surface area, procedure and calculation of photonic efficiency, XRD patterns of {001} BiOCl NS before and after photodegradation, recycling test for phtodegradation of RhB, Fitting parameters for time resolve PL decay curves can be found in supplementary information. See DOI: 10.1039/x0xx00000x

View Article Online
DOI: 10.1039/C6CP01740A

and hydrothermal[16,21] methods. BiOCl has shown better photodegradation ability compared to commercial TiO_2, Degussa P25.[26] Crystal facet engineering of BiOCl is promising strategy to improve its photocatalytic ability[16,27-31] EPR investigation has shown that oxygen vacancies generated across {001} facet under UV irradiation are accountable for improved performance.[26] Another finding has revealed that photocatalytic activity of {001} facet is much higher compared to {010} facet of BiOCl.[16] DFT calculations have further suggested that surface energy of {001} facet, $\gamma_{001\text{-}O}$, *ca*. 2.42 $J.m^{-2}$ is much higher compared to {010} facet, $\gamma_{001\text{-}O}$, *ca.* 0.51 Jm^{-2}.[27] Recently {001} BiOCl has been applied for PEC water splitting[32], CO_2 photoreduction[33] as well as organic transformations.[29]

Well defined morphology of exposed crystal facets is essential for realizing optimum performance. Previous work reported in literature describes either formation of uncontrolled morphologies[26] or it involves the use of organic surfactants such as PVP[28] or oleic acid[29]. Organic surfactants may alter surface properties such as hydrophilicity,[29] which can possibly influence on surface adsorption during photocatalytic reactions. Organic surfactants can be preferentially adsorbed on the reactive crystals facets. Acting as a trapping site they can promote recombination of electron and hole pairs resulting in inferior performance.[34] Therefore, post synthesis additional steps such as thermal annealing,[35] UV irradiation[36] and chemical treatement[37] are frequently described in literature to get rid of these organic surfactants adhered on the surface of nanocrystals. Moreover existing reports in the literatures for fabricating {001} BiOCl are mainly devoted to either three dimensional spherical structure or two dimensional square plates. Whereas octagonal shaped {001} faceted BiOCl has been rarely discussed in literature.[38,39]

Hence it would be appropriate to work out simplified route to fabricate unique morphology of BiOCl particles with {001} crystal facet exposed BiOCl without using organic surfactants. However, it has been quite challenging, since such attempts usually results in production of random shape of BiOCl particles. Herein this work a facile hydrothermal route has been explored to prepare octagonal shaped {001} BiOCl nanosheets (NS) without using organic surfactants. As prepared {001} BiOCl NS have shown superior charge transportation properties, suppressed recombination of electron and hole pairs and longer lifetime of photoinduced charge carriers. Moreover, {001} BiOCl NS demonstrated significant enhancement in photocatlytic activity with higher photonic efficiency. Mechanism for photodegradation of RhB was investigated in detail to find out the role of active species involved in efficient removal of RhB.

Experimental

Materials and Chemicals

Bismuth triiodide, (BiI_3, 99%), anhydrous ethanol (C_2H_5OH, 99.99%), bismuth nitrate pentahydrate ($Bi(NO_3)_3{\cdot}5H_2O$, 98%), p-benzoquinone (BQ, 98%) and potassium chloride (KCl, 99%) were purchased from Sigma Aldrich, rhodamine B (RhB) from Aldrich Chemicals, hydrochloric acid (HCl, 36.6%), triethnaolamine (TEA, 90 %) and isoproponal (IPA, 99.5%) were obtained from Samchun Chemicals. All reagents were used as supplied. Deionized (DI) water was obtained from Millipore system.

Preparation of {001} BiOCl NS

In a typical synthesis, 0.044 g of BiI_3 was transferred to 3.0 ml of absolute ethanol in a glass vial. To this mixture, 20 µl of concentrated HCl (36.6%) was added by drop wise. Mixture was magnetically stirred until a transparent red colored solution was obtained. To this solution 12 ml of DI water was added under vigorous stirring for 10 min. The clear solution was precipitated with sudden appearance of turbidity. Reaction mixture was transferred to a teflon lined stainless steel autoclave (volume capacity, 30 ml) and heated in an electric oven at 180 ^{o}C for 4 h. The product was separated by centrifuge and washed several times with ethanol and DI water. Finally it was vacuum dried at 60 ^{o}C for 10 h.

Preparation of Pristine BiOCl

Pristine BiOCl particles were prepared by a modified reported procedure.[16] For the sake of comparison hydrothermal duration (4 h) and temperature (180 ^{o}C) were kept similar to that of {001} BiOCl NS. Briefly, 1.0 mmol (0.48507 g) of $Bi(NO_3)_3.5H_2O$ was dispersed in 15 ml of DI water under stirring. A milky suspension was produced, 1.0 mmol (0.0745 g) of KCl was added to it and stirring was continued for another 15 min. Mixture was heated at 180 ^{o}C for 4 h, white precipitates were recovered and vacuum dried at 60 ^{o}C for 10 h.

Characterization

Various experimental techniques were adopted for characterization of samples. Crystal structure of samples was analyzed by X-ray diffractometer (Rigaku miniFlex-II) equipped with Cu Kα radiation (λ = 0.154056 nm). The morphology was observed by scanning electron microscope (SEM, Hitachi S-4300) and transmission electron microscope (TEM, JEM 2100-F). Chemical composition was monitored by energy dispersive X-ray spectroscopy (EDX) analysis. Diffuse reflectance spectra, Tauc plot and UV-Visible absorption spectra were obtained with UV-Vis-NIR Spectrophotometer (Cary 5000, Agilent Technologies). BET surface area measurement was carried out by nitrogen adsorption/desorption isotherms using Autosorb-1 (Quantachrome Instruments.). Chemical states of elements were identified by X-ray photoelectron spectrum (XPS) using XPS instrument (MultiLab 2000). Photoluminescence spectra were measured by F-700 spectrophotometer (Hitachi). Average lifetime of excited charge carriers was measured by MicroTime-200 (Pico Quant), equipped with 375 nm laser excitation source and monitoring wavelength range of 450 nm to 690 nm at Korea Basic Science Institute (KBSI). Wavelength dependent output irradiance of light source was measured by Sp4-03 spectroradiometer (Luzchem).

Photocatalytic and Photoelectrochemical Evaluation

Photocatalytic activity of {001} BiOCl NS and pristine BiOCl were measured by photodegradation of organic dye, RhB, under visible light irradiation. For checking photoactivity, 40 mg of catalysts were dispersed into 60 ml of 20 ppm RhB solution in a quartz reactor. It was stirred in dark for 1 h to achieve adsorption/desorption equilibrium. The reaction mixture was irradiated with visible light using 300 W Xenon

View Article Online
DOI: 10.1039/C6CP01740A

lamp (Max 302, Asahi Spectra, Japan) equipped with 400 nm long pass filters. Radiation intensity from 400-600 nm was observed as 14.67mW/cm^2. After regular intervals of illumination an aliquot of 5 ml was withdrawn from reaction mixture and catalyst was separated from dye solution by centrifugation at 9000 rpm for 8 min. The decrease in dye concentration as a function of irradiation time was monitored by measuring decrease in optical absorption of RhB. For comparison, photocatalytic activity of pristine BiOCl was also measured under identical conditions. Photodegradation mechanism was explored by finding active species involved in decomposition of RhB. 1.5 mM of IPA, BQ and TEA were used for quenching agents of hydroxyl radicals (OH^-), superoxide radicals ($^{\cdot}O^{2-}$) and photogenerated holes (h^+), respectively.

Photoeclectrochemical (PEC) measurements were performed in three electrodes cell, a working electrode, pt wire as counter electrode and Ag/AgCl as reference electrode at 0.5 V in 0.5 M Na_2SO_4 aqueous solution as electrolyte under illumination of 1 Sun (100 mw/Cm^2). Working electrode was prepared by following a reported procedure.[16] Typically, 2.5 x 2.5 cm measuring of fluorine doped tin oxide (FTO) as a conducting substrate was cleaned by successive ultrasonication in DI water, acetone and ethanol. Then it was dried by blowing N_2 gas. A 20 mg of BiOCl sample was dispersed in 40 µl of PEDOT:PSS (1.3 weight% in water, conductive grade, Sigma Aldrich) and 200 µl of DI water. The paste was dispersed on cleaned FTO glass, dried and then annealed in an electric oven at 150 ^{o}C for 10 minutes. Charge transfer properties of electrodes were further investigated by measuring electrochemical impedance spectroscopy (EIS) under dark and illumination using 0.5M Na_2SO_4 aqueous solution as electrolyte. Measurement was performed at open circuit potential (OCP) with a frequency range of 0.01-10^5 Hz.

Results and Discussions

SEM images of {001} BiOCl NS shown in Figure 1 (a, b) indicate the formation of monodisperse nanosheet structures with uniform dispersion. Elemental mapping given in the Figure S1(a) reflects that in-situ iodine was doped into {001} BiOCl NS with uniform dispersion. EDX analysis (Figure S1(b)) confirms the presence of 0.46 wt% of iodine to {001} BiOCl NS. TEM images (Figure 1 (c, d)) indicate that as formed {001} BiOCl NS is composed of eight corners having octagonal morphology. Most of the previous work have been devoted to square shaped BiOCl,[28-30] three dimensional hierarchical structures, or uncontrolled morphologies[16,21,26,38,39] However, this work describes fabrication of octagonal shaped {001} faceted BiOCl NS without using organic surfactants. Thickness of {001} BiOCl NS calculated from vertically standing NS was around 41 nm (Figure 1(e)-(f)). Appearance of ordered bright fringes in the SAED pattern (Figure 1(g)) indicates that as prepared sample is well crystalline in nature. The angle between (110) and (200) crystallographic planes was 45^{o}, confirming exposed {001} crystal facet of {001} BiOCl NS.[16] HRTEM image given in Figure 1(h) reflects clear lattice fringes and inter-planar distance of d = 0.278 nm was assigned to (110) crystal plane of BiOCl.[28] Exposed {001} facet and c-axis growth of {001} BiOCl NS are represented by model given in Figure 1(i). Three dimensional crystal structure of {001} BiOCl NS and projection across {001} plane are given in Figure S2. SEM images of pristine BiOCl given in Figure 2(a)-(b) indicates formation of uncontrolled squared shape of BiOCl particles. Thickness of pristine BiOCl around 197 nm was appeared to be much higher compared to

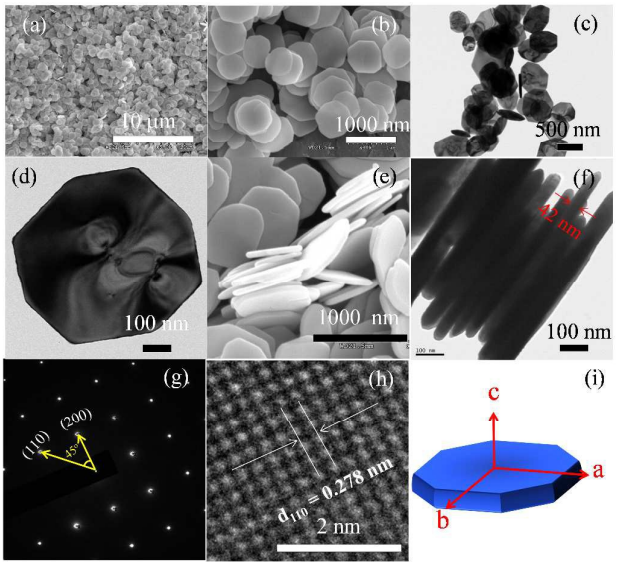

Figure1: SEM images (a, b), TEM images (c, d of {001} BiOCl NS; SEM image (e), TEM image (f) of vertically standing NS, SAED pattern (g), HRTEM image (h) of {001} BiOCl NS and schematic illustration of {001} facet orientation (i).

{001} BiOCl NS such as 41 nm. It is presumed that smaller thickness of {001} BiOCl NS can facilitate rapid migration of photogenerated electron and hole pairs to the surface, where they can actively take part in surface redox reaction during photocatalysis.[40]

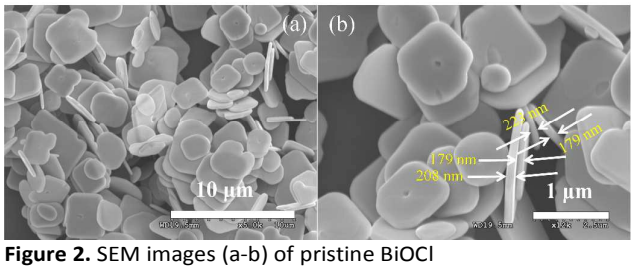

Figure 2. SEM images (a-b) of pristine BiOCl

Percentage exposure of {001} facet was calculated by applying geometric model as shown in Figure S3. SEM images of {001} BiOCl NS and pristine BiOCl referred for calculations of exposed facets are given in Figure S4(a) and Figure S4(b) respectively. {001} facet exposure for {001} BiOCl NS observed as 88.4% is higher compared to pristine BiOCl, 82.5%. Since theoretical findings have suggested that surface energy of {001} facet of BiOCl is much higher as compared to {010} facet.[27] Therefore, larger exposure of high energy facet of {001} BiOCl NS as compared to pristine BiOCl is favourable for higher photocatalytic activity.

XRD patterns of {001} BiOCl NS and pristine BiOCl are shown in Figure 3 (a). All of the diffraction peaks belong to tetragonal crystal structure of BiOCl, and matches well to standard JCPDS pattern no. 06-0249. Absence of any extra peak reflects single crystalline nature and phase purity of as prepared samples.

View Article Online
DOI: 10.1039/C6CP01740A

High peak intensity of (001) BiOCl crystal facet family reflected predominant exposure of {001} crystal facet[38] and this is in agreement with SAED pattern (Figure 1(g)).

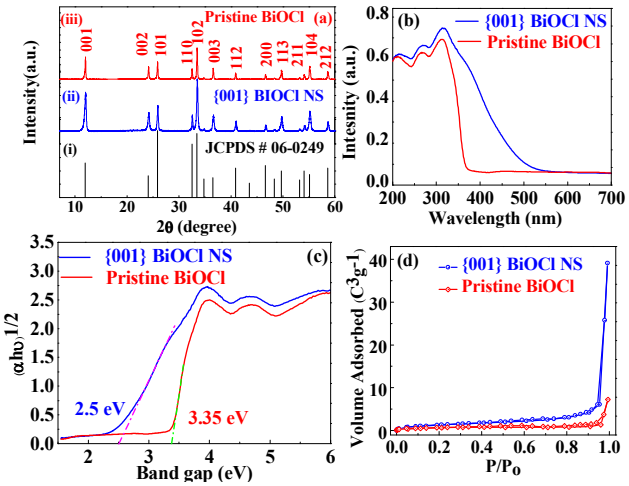

Figure 3. XRD patterns (a), UV-Visible diffused reflectance spectra (b), Tauc plots (c) and nitrogen adsorption-desorption isotherms (d) of {001} BiOCl NS and pristine BiOCl.

It is important to understand mechanism for growth of {001} BiOCl NS. Since Bi^{3+} ions are readily precipitated in aqueous environment,[37] variety of organic surfactants are conventionally applied for controlling morphology of {001} crystal facet exposed BiOCl nanoparticles.[28-29] In this work optimized solvent ratio of ethanol and DI water played an important role for the controlled fabrication of {001} BiOCl NS. BiI_3 was dissolved in HCl containing absolute ethanol to produce transparent red solution. Non aqueous and acidic environment prevented rapid precipitation of Bi^{3+}. Slow addition of DI water increased turbidity due to formation of BiOCl nuclei in the reaction bath. Excess of I^- and Cl^- ions both were present in the reaction mixture, however, stronger electronegativity enabled favourable attractions between positively charged $[Bi_2O_2]^+$ slabs and negatively charged Cl^- anions producing BiOCl. Smaller fraction of I^- was introduced as a dopant. Acidic protons (H^+) in reaction mixture were responsible for anisotropic growth of BiOCl NS along c-axis.[16]

In order to investigate possible influence of solvent ratio on the growth of {001} BiOCl NS, hydrothermal reactions were performed by varying volume proportion of ethanol and DI water. With a fixed total volume of 15 ml, different volume ratios of ethanol/DI water such as 14/1, 11/4, 6/9, 4/11, 3/12, 2/13 and 1/14 ml were tested. Using higher ethanol ratio compared to DI water such as ethanol/DI water, 14/1 ml and 11/4 ml, no hydrothermal product was formed at all. BiI_3 solution remains clear and transparent at the end of reaction. It was due to insufficient hydrolysis of BiI_3 under such conditions. Reducing ethanol in case of ethanol/DI water, 6/9, 4/11 ml resulted in appearance of micro-sized particles along with NS as shown in Figure S5((a)-(b)). It was due to suppression in nucleation of BiOCl due to high amount of ethanol in reaction mixture. Ethanol/DI water of 3/12 ml was observed as optimized condition for controlled morphology of {001} BiOCl NS (Figure 1(a)-(f)). Further lowering of ethanol proportion such as ethanol/DI water, 2/13 and 1/14 ml can get rid of micro-sized plates in the product, however, morphologies of NS remains uncontrolled as shown in Figure S5((c)-(d)). It was due to sudden hydrolysis of BiI_3 under such conditions. For further exploring growth mechanism to evaluate the significance of Bi^{3+} source on nanosheet morphology, additional hydrothermal experiments were conducted by replacing BiI_3 with $Bi(NO_3)_3.5H_2O$ and $BiCl_3$ while keeping solvent ratio (ethanol/Di water, 3/12 ml) and amount of HCl (20 μl) constant. XRD patterns and morphologies of corresponding samples are presented in Supporting Information Figure S6 and Figure S7, respectively. Figure S6 confirmed that their crystal structure remained same regardless of various Bi^{3+} precursors. SEM images presented in Figure S7 indicated that $Bi(NO_3)_3.5H_2O$ and $BiCl_3$ both of them have produced two dimensional nanosheet structures. However, morphologies of nanosheets remained random and uncontrolled. It is suggested that uncontrolled shape of particles are appeared due to rapid and uncontrolled hydrolysis of Bi^{3+} under such conditions. Figure 1 and Figure S7 confirmed that morphology of {001} BiOCl NS is significantly affected by Bi^{3+} precursors. Influence of Iodine source on morphology was also studied by adding NaI and KI in the reaction system during hydrolysis of $Bi(NO_3)_3.5H_2O$ and $BiCl_3$. It is suggested that formation of random morphologies from $KI+Bi(NO_3)_3.5H_2O$, $NaI+Bi(NO_3)_3.5H_2O$, $KI+BiCl_3$ and $NaI+BiCl_3$ (Figure S7) were mainly due to uncontrolled hydrolysis of Bi^{3+} cations released from $Bi(NO_3)_3.5H_2O$ and $BiCl_3$ and morphologies are less likely dependent upon iodine source such as NaI or KI. Above discussion clarifies that choice of suitable Bi^{3+} precursor and optimized solvent ratio both are indispensable for controlled hydrolysis of Bi^{3+} to realize uniform growth {001} BiOCl NS. This approach can be potentially extended for crystal facet engineering of other bismuth based semiconductors. Further investigations on this subject are currently underway and will be reported elsewhere.

Diffused reflectance spectroscopy provides convenient way to examine optical properties. Bandgap can be calculated from Tauc plot using following equation, $(\alpha h\nu)^{\frac{1}{n}} = B(h\nu - E_g)$.[41] In above expression the values of α, h, ν, Eg, and B represent absorption co-efficient, plank's constant, frequency, bandgap and proportionality constant, respectively. The value of n in the exponent is 2 for BiOCl.[41] Absorption spectra and Tauc plots are given in Figure 3(b)-(c). {001} BiOCl NS shows strong absorption in the visible region and its absorption end is extended to 530 nm. Bandgap of {001} NS is calculated as 2.5 eV. Introduction of I^- has enabled extended absorption in the visible range and shortening of bandgap. However, pristine BiOCl reflects entire absorption in the UV region with a wide bandgap of 3.35 eV, in line with typical response of BiOCl referred in literature.[16] Extended absorption of {001} BiOCl NS compared to pristine BiOCl can promote its photocatalytic activity under visible light irradiation. BET surface area values can directly influence on photocatalytic activity.[42] Larger surface area can improve activity of photocatalyst.[11] Surface area of two dimensional nano structures can be tuned by varying size and thickness of nanosheets. Therefore surface area of {001} BiOCl NS and pristine BiOCl were examined. Figure 3(d) represent N_2 adsorption/desorption isotherms,

View Article Online
DOI: 10.1039/C6CP01740A

whereas calculated values of surface area are summarized in Table 1. BET surface area of {001} BiOCl and pristine were calculated as 5.53 m^2g^{-1} and 2.44 m^2g^{-1}, respectively. Higher surface area of {001} BiOCl NS as compared to pristine BiOCl is quite obvious considering their size and thickness. Smaller thickness and lower size of {001} BiOCl NS across lateral dimensions are accountable for higher surface area, which is presumed to have favourable contribution in a higher performance during photocatalysis.

Chemical states of elements were identified by XPS analysis. Figure 4(a) represents XPS survey spectrum of {001} BiOCl NS and shows the presence of Bi, Cl, O, I and C.[43] Figure 4(b) shows Bi 4f spectrum of {001} BiOCl NS. Appearance of characteristic peaks at binding energies of 161.2 eV and 166.5 eV is assigned to Bi $4f_{7/2}$ and Bi $4f_{5/2}$.[43] Appearance of two additional peaks at lower binding energies of 159.5 eV and 165.2 eV are assigned to Bi^{3+} indicating presence of surface oxygen vaccancies.[44] These surface oxygen vacancies are probably formed by the interaction of oxygen terminated BiOCl with ethanol during hydrothermal synthesis.[21] Previous findings have suggested that oxygen vacancies are favorable for enhancing visible light photocatalytic activity of BiOCl.[26] Presence of iodine in the sample is confirmed by I 3d spectra as shown in the Figure 4(c). Appearance of characteristic peaks at binding energies of 621 eV and 632.5 eV are identified as I $3d_{5/2}$ and I $3d_{3/2}$.[46] Pristine BiOCl does not show the presence of iodine in the sample as evident from Figure 4(d). Cl 2p spectrum (Figure 4(e) indicated appearance of two peaks at binding energy values of 197 eV and 200 eV, which are assigned to Cl $2p_{3/2}$ and Cl $2p_{1/2}$.[41] O1s spectrum (Figure 4(f) is de-convoluted into two major peaks at binding energies of 529.2 eV and 533.6 eV, which are assigned to O1s of Bi-O and O1s of H-O, respectively.[45] Lifetime of charge carriers is essential to consider for designing highly efficient photocatalyst. Due to very fast recombination tendency, electron and holes pairs are recombined within nanoseconds. Rational design of photocatalyst with improved dynamics of charge carriers could be a promising strategy to improve efficiency. Lifetime of photoexcited carriers are probed by time resolved fluorescence decay studies as shown in Figure 5. The average lifetime can be expressed either as amplitude weighted $<\tau>_{amp.}$[47] or intensity weighted $<\tau>_{int.}$[48] both of them have been frequently referred in literature. $<\tau>_{amp.}$ and $<\tau>_{int.}$ were calculated by following expression.[47-48]

$$<\tau>_{int.} = \sum_{i=1}^{3} B_i \tau_i^{\,2} \Big/ \sum_{i=1}^{3} B_i \tau_i$$

$$<\tau>_{amp.} = \sum_{i=1}^{3} B_i \tau_i \Big/ \sum_{i=1}^{3} B_i$$

Fitting parameters for PL decay curves are summarized in Table S1. {001} BiOCl NS demonstrates elongation in the lifetime of carriers (Table 1). $<\tau>_{int.}$ and $<\tau>_{amp.}$ of {001} BiOCl NS were observed as 17.23 ns and 1.94 ns, respectively. These are sufficiently high as compared to corresponding values for pristine BiOCl such as 2.52 ns and 1.07 ns. Improvement in the lifetime of charge carrier reflects better electron transport properties of {001} BiOCl NS. Such improvement in the dynamics of carriers without formation of homo or heterojunction is quite interesting.[49] Smaller thickness of {001} BiOCl NS compared to pristine BiOCl is found favourable for efficient transportation and separation of charge carriers. It enables reduced path length for transportation of charge carriers. They can quickly move to surface of {001} BiOCl NS before getting recombined, where they can participate in photocatalytic reactions.

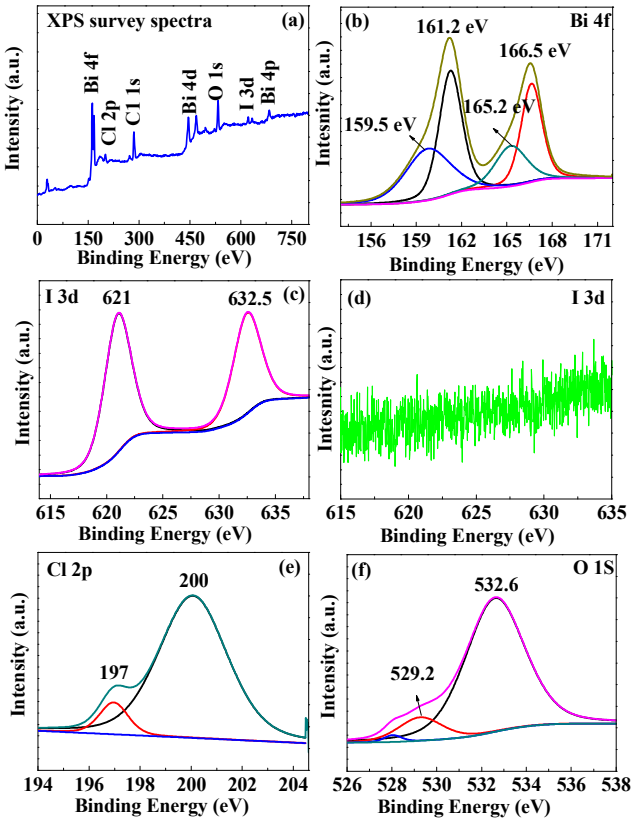

Figure 4. XPS survey spectra (a), Bi 4f (b), I 3d (c) of {001} BiOCl NS, I 3d (d) of pristine BiOCl, Cl 2p (e) and O 1s (f) of {001} BiOCl NS.

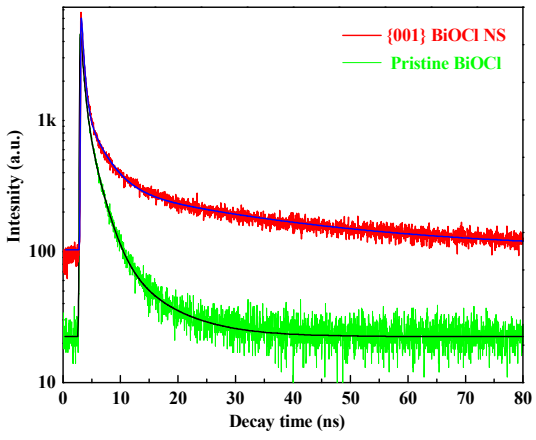

Figure 5. Time resolved photoluminescence decay spectra

View Article Online
DOI: 10.1039/C6CP01740A

In contrast, much larger thickness of pristine BiOCl can favour recombination of majority of charge carriers in bulk of pristine BiOCl before getting arrived to its surface. It promotes recombination with simultaneous shortening in the lifetime of charge carriers. Under such conditions fewer numbers of carriers are available on the surface of pristine BiOCl for photocatalysis. Role of thickness on the lifetime of carriers is highlighted in schematic diagram (Figure 6).

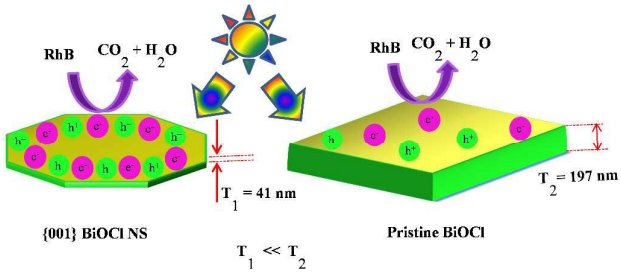

Figure 6. Schematic diagram for transportation of charge carriers on the surface of {001} BiOCl NS and pristine BiOCl

Size dependent variation in dynamics of charge carriers is supported by previous findings reported in literature.[40,50] Nanoparticle thickness has been reported to have critical influence on quantum yield, space charge width and diffusion length of charge carrier.[51-52] Lifetime and diffusion coefficient are correlated by following expression, $L_n = (D_nT_n)^{1/2}$.[53] In this expression, T_n reflects lifetime of carriers, D_n denotes diffusion coefficient and L_n reflects diffusion length. It is suggested that if the size or thickness of nanoparticles is comparable or less than diffusion coefficient, it could realize exceptionally high charge collection efficiencies.[51-53] Above discussion supports that reduced thickness of {001} BiOCl NS compared to pristine BiOCl is favourable for extending lifetime of photoinduced charge carriers. Photoluminescence (PL) spectroscopy provides a convenient way to analyze recombination tendencies of electron and hole pairs.[54] PL spectra given in Figure 7(a) indicates appearance of two peaks at 382 nm and 469 nm, designated as typical emission bands of BiOCl. PL spectra of {001} BiOCl NS demonstrates significant quenching in PL emission intensity compared to pristine BiOCl. It confirms that {001} BiOCl NS has lower recombination tendency compared to pristine BiOCl. This observation is in agreement with PL decay trend as shown in Figure 5. In order to find out the contribution of iodine doping in quenching PL emission intensity, controlled samples of pristine BiOCl were prepared by introducing different percentage of iodine such as 0.5%, 1.0% (iodine % is based on initial amount of I/Bi sources). PL emission spectra indicate a positive correlation between iodine contents and quenching of PL emission intensity. Similar strategy of in-situ iodine doping has demonstrated to minimize recombination of electron and hole pairs in graphitic carbon nitride.[55] Figure 7(a)-(b) reveals following order in recombination rate of photo induced charge carriers, {001} BiOCl NS < BiOCl 0.5%I < BiOCl 1.0 % < pristine BiOCl. Although doping of iodine to pristine BiOCl is favorable to suppress recombination, however, extended separation of charge carriers for {001} BiOCl NS is promoted due to contribution of both iodine doping as well as favourable thickness.

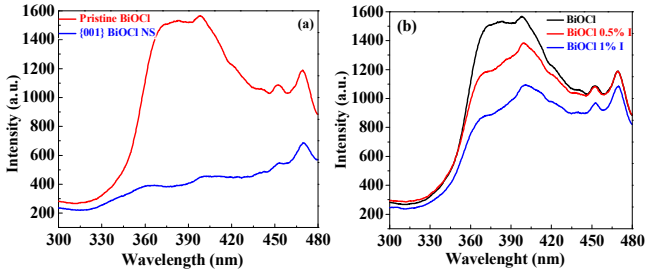

Figure 7. PL spectra of {001} BiOCl NS and pristine BiOCl (a) and different weight percent of iodine doped BiOCl.

Above discussion clarifies that smaller thickness and in-situ iodine doping were responsible for significant improvement in the dynamics of photoexcited charge carriers by increasing average lifetime of charge carriers. $\langle\tau\rangle_{int.}$ and $\langle\tau\rangle_{amp.}$ of {001} BiOCl NS such as 17.23 ns and 1.94 ns is higher than corresponding values of pristine BiOCl such as 2.52 ns and 1.07 ns. Such observation is in agreement with reduced recombination of charge carriers as observed by photoluminescence spectroscopy.

Photocatalytic activity of as prepared samples was studied by photodegradation of RhB under visible irradiation (λ > 400 nm). A 300 W Xenon lamp equipped with 400 nm long pass filter was used as a source of irradiation. Spectral irradiance of incident radiation is shown in the Figure S8. Before illumination of light, catalyst and dye solution were stirred under dark for 1 h to establish adsorption/desorption equilibrium. Decrease in concentration of RhB was monitored by plotting C/C_o versus time. C denotes concentration of RhB at certain time intervals and C_o indicates original concentration of RhB at initial. Efficiency for photodegradation of RhB was calculated according to following expression.

$$\eta\,(\%) = \frac{C_0 - C}{C_0} \times 100$$

Figure S9 shows that {001} BiOCl NS and pristine BiOCl adsorbed 11.2% and 4.8% of RhB under dark. It is negligible compared to photodegradation under light. Figure 8(a) reflects that after 2 h of Illumination, {001} BiOCl NS and pristine BiOCl showed 61.7% and 22% of photodegradation efficiency. Removal of RhB under irradiation in absence of catalyst is negligible. Absorption spectra of RhB under dark and under illumination are given in Figure S10. For comparison of photocatalytic activity rate constant of reaction was calculated by following expression.

$$-\ln\frac{C}{C_0} = K_{app}t$$

Figure S11(a) shows liner plot of $1n(C/C_o)$ versus time, it reflects pseudo first order reaction. Rate constant for BiOCl NS K_a, 0.008 min^{-1} was found to be 4 times higher compared to rate constant for pristine BiOCl K_b, 0.002 min^{-1} (Figure 8(b)). Rate constant for {001} BiOCl NS normalized to BET surface area K_c, 0.0014 gm-2min^{-1} is also 1.5 times higher compared to that of pristine BiOCl, K_d, 0.0008 gm-2min^{-1}. (Figure S11(b) For brief evaluation of photocatalytic activity, it is important to consider photonic efficiencies (PE) of photodegradation of

View Article Online
DOI: 10.1039/C6CP01740A

RhB. Considering flux of incident radiation and photodegradation of RhB, Photonic Efficiency was calculated by following expressions.[56]

$$\varphi(\%) = \frac{d[x]/dt}{d[hv]/dt} \times 100$$

In above expression $d[x]/dt$ is photodegradation rate of RhB, $d[hv]/dt$ represents incident photons on the sample. Detailed procedure adopted for calculations of PE has been summarized in Figure S12. Observed PE values for {001} BiOCl NS of 0.0486 is much higher compared to PE of pristine BiOCl of 0.0173. Above discussion clarifies that {001} BiOCl NS has demonstrated superior activity compared to pristine BiOCl.

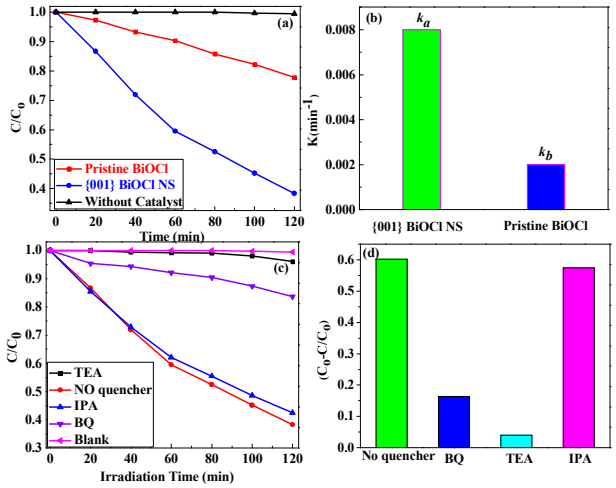

Figure 8. Photodegradation of RhB under visible light irradiation (a), rate constant for photodegradation of RhB by {001} BiOCl NS and pristine BiOCl (b) and effect of quenching

{001} BiOCl NS has shown better activity in term of rapid photodecomposition of RhB, higher rate constant of reaction normalized to BET surface area, as well as higher response for photonic efficiency. Higher activity of {001} BiOCl NS is mainly assigned due to improvement in the charge carrier's lifetime, minimized recombination of electron-hole pairs as well as enhanced absorption in visible region. Stability and reusability of {001} BiOCl NS was confirmed by no change in XRD pattern after photodegradation and recycling tests as shown in Figure S13. As apparent from diffused reflectance spectra given in Figure 3(b), pristine BiOCl cannot be excited under visible irradiation. Hence, visible light photodegradation of RhB by pristine BiOCl is preceded via indirect photosensitization pathway.[16] However, due to extended absorption in the visible region {001} BiOCl NS as well as RhB both of them can get excited upon visible light irradiation. Photodegradation of RhB under such condition is due to combined effect of direct bandgap photoexcitation as well as photosensitization of RhB. It is clear that in-situ iodine doping to {001} BiOCl NS has influenced on optical absorption and photocatalytic mechanism when compared to undoped pristine BiOCl. However, comparing both of these samples provided useful information about structure-property relation. It enabled to figure out the critical role of iodine doping on charge carrier dynamics, lifetime of carriers, quenching PL emission intensity and minimizing recombination tendency of electron and hole pairs. Iodine doping induced enhanced optical absorption, long live charge carriers and suppression in recombination had important contribution to enhance photocatalytic activity of {001} BiOCl NS. Mechanism for photodegradation of RhB by {001} BiOCl NS was explored by using various quenchers. Photodegradation mechanism and participation of active species in photodegradation of RhB have been illustrated in the schematic diagram given in Figure 9. Figure 8((c)-(d)) shows that photodegradation of RhB was significantly quenched in presence of triethanol amine (TEA) used as a hole (h^+) scavenger.[57-58] It reflects that photogenerated holes played active role for photodegradation of RhB. Para benzoquinone (BQ) was employed as superoxide radical ($\cdot O^{2-}$) generated via oxygen reduction reaction through CB electrons. Figure 8(c) shows that considerable quenching of RhB in presence of BQ. It reflects that superoxide radicals have also played important role in photodegradation of RhB.[57] However, a slight decrease in photoactivity upon addition of isopropyl alcohol (IPA) indicates that hydroxyl (OH^-) has the least contribution in photodegradation of RhB.[58] Active species involved in reactions have following order, photogenerated holes > superoxide radicals > hydroxyl radical.

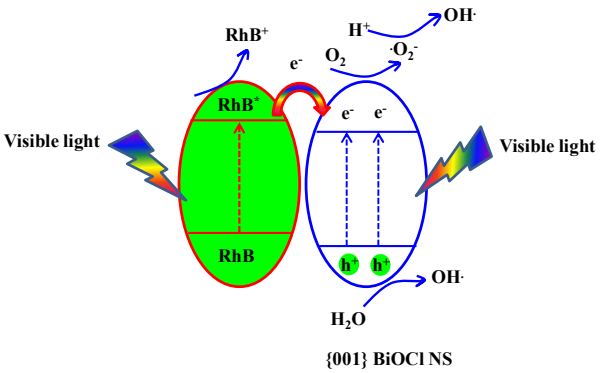

Figure 9. Mechanism for visible light photodegradation of RhB on {001} BiOCl NS.

Photocurrent measurement provides a convenient way to analyze separation and transfer of photogenerated charge carriers. Hence, transient photocurrent response of {001} BiOCl NS and pristine BiOCl were measured by fabricating respective electrodes on FTO as a conducting substrate. "*It*" curves given in Figure 10(a) show time dependent on-off cycles of photocurrent generation. Diminishing of photocurrent upon turning off light clearly indicates that photocurrent is produced by irradiation. Higher photocurrent density of {001} BiOCl NS reflects higher degree of separation and better collection efficiency of charge carriers. It improved photoelectrochemical performance of {001} BiOCl NS. For better understanding of charge transfer capabilities, {001} BiOCl NS and pristine BiOCl electrodes were further studied by electrochemical impedance spectroscopy (EIS). Nyquist plots of samples presented in Figure 10(b) reveals lower charge transfer resistance for {001} BiOCl NS as compared to pristine BiOCl. It favoured generation

View Article Online
DOI: 10.1039/C6CP01740A

of higher photocurrent density. Improved photocurrent response and inferior charge transfer resistance are consistent with superior photocatalytic activity of {001} BiOCl NS for degradation of RhB as shown in Figure 8. Above discussion confirms enhanced photocatalytic activity of {001} BiOCl NS.

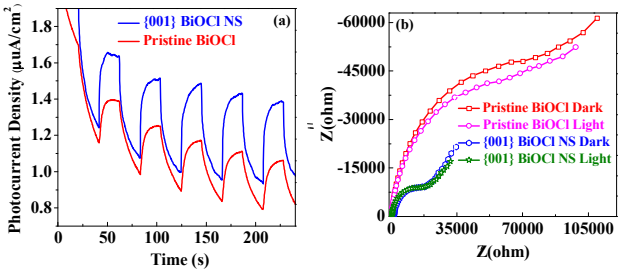

Figure 10. Transient photocurrent density vs time measured at 0.5 V in 0.5 M Na_2SO_4 (a) and Electrochemical impedance Nyquist plot under light and dark (b) of {001} BiOCl NS and pristine BiOCl.

To summarize, {001} BiOCl NS has shown significant improvement in photodegradation of RhB under visible illumination. Rapid degradation kinetics, higher rate constant for photodegradation as well as superior photonic efficiency were observed. Several features were supportive to enhance photocatalytic activity of {001} BiOCl NS such as favourable thickness, in-situ iodine doping, high BET surface area, large percentage of exposed {001} crystal facets as well as synergetic effect of direct and indirect photoexcitation. However, among these factors in-situ iodine doping has played an important role. It was directly helpful to improve photocatalytic (Figure 8) and photoelectrochemical (Figure 10) performance of {001} BiOCl NS by extending optical absorption in visible spectrum (Figure 3(b, c)), increasing lifetime (Figure 5, Table 1, Table S1) and reduced recombination of charge carriers (Figure 7).

Table 1. Summary of photodegradation efficiency, BET surface area, photonic efficiency and lifetime of excited charge carriers.

Sample	Degradation Efficiency, η (%)	BET (m^2g^{-1})	PE (%)	$<\tau>_{int}$	$<\tau>_{amp}$
{001} BiOCl NS	61.7	5.53	0.0486	17.23	1.94
Pristine BiOCl	22	2.44	0.0173	2.52	1.07

Conclusion

Fabrication of unique octagonal shaped BiOCl NS with dominant exposure of high energy {001} facets has been realized without using organic surfactants as structure directing agents. As prepared {001} BiOCl NS exhibited enhanced separation of photoexcited charge carriers. Reduced thickness and introducing iodine as a dopant to high energy facet supported to realize long lived charge carrier, resulting significant improvement in their average lifetime. {001} BiOCl NS revealed significant improvement in visible light photocatalytic activity when compared to pristine BiOCl. Several order increase in photodegradation of RhB and improvement in photonic efficiency was observed. Photocatalytic mechanism of {001} BiOCl NS was thoroughly investigated with the help of various quenching agents. It was revealed that photogenerated holes (h^+) and superoxide radicals ($^{\cdot}O^{2-}$) actively participated whereas hydroxyl ($OH^{\cdot}$) radicals have negligible contribution in photodegradation of RhB. This study may offer new opportunities for tailoring charge carrier dynamics of high energy facets to design highly efficient photocatalyst.

Acknowledgements

This research was supported by the Korea Center for Artificial Photosynthesis (KCAP) located in Sogang University (No. 2009-0093885) funded by the Ministry of Science, ICT and Future Planning (MSIP) through the National Research Foundation of Korea and the Brain Korea 21 Plus Project 2015. Authors would like to thank Professor Detlef Bahnemann for useful discussion about photonic efficiency.

Notes and References

1 H. G. Yang, C. H. Sun, S. Z. Qiao, J. Zou, G. Liu, S. C. Smith, H. M. Cheng, G. Q. Lu, *Nature*, 2008, **453**, 638.
2 F. Liao, Y. Huang, J. Ge, W. Zheng, K. Tedsree, P. Collier, X. Hong, S. C. Tsang, *Angew. Chem. Int. Ed.,* 2011, **50**, 2162.
3 Y. Zhao, F. Pan, H. Li, T. Niu, G. Xu, W. Chen. *J. Mater. Chem. A.,* 2013, **1**, 7242.
4 D. F. Zhang, H. Zhang, L. Guo, K. Zheng, X. D. Han, Z. Zhang. *J. Mater. Chem.,* 2009, **19**, 5220.
5 Y. P. Xie, G. Liu, L. Yin, H. M. Cheng. *J. Mater. Chem., 2012*, **22**, 6746.
6 R. Li, F. Zhang, D. Wang, J. Yang, M. Li, J. Zhu, X. Zhou, H. Han, C. Li, *Nature Commun*., 2013, **4**, 1432.
7 H. G. Cha, M. J. Kang, I. C. Hwang, H. Kim, K. B. Yoon, Y. S. Kang, *Chem. Commun*., 2015, **51**, 6407.
8 C. W. Kim, Y. S. Son, M. J. Kang, D. Y. Kim, Y. S. Kang, *Adv. Energy Mater*., 2015,1501754.doi:10.1002/aenm .2015 01754.
9 A. U. Pawar, C. W. Kim, M. J. Kang, Y. S. Kang, *Nano Energy,* 2016, **20**, 156.
10 C. W. Kim, S. J. Yeob, H. M. Cheng, Y. S. Kang, *Energy Environ. Sci.,* 2015, **8**, 3646.
11 J. Y. Zheng, Z. Haider, T. K. Van, A. U. Pawar, M. J. Kang, C. W. Kim, Y. S. Kang. *CrystEngComm*., 2015, **17**, 6070.
12 A. P. Kaushik, B. Lukose, P. Clancy, *ACS Nano*, 2014, **8** (3), 2302.
13 N. Erdman, K. R. Poeppelmeier, M. Asta, O. Warschkow, D. E. Ellis, L. D. Marks, *Nature*, 2002, **419** 55.
14 B. Lv, Z. Liu, H. Tian, Y. Xu, D. Wu, Y. Sun, *Adv. Funct. Mater*., 2010, **20**, 3987.
15 W. Liu, J. G. Wang, W. Li, X. Guo, L. Lu, X. Lu, X. Feng, C. Liu, Z. Yang, *Phys. Chem. Chem. Phys.,* 2010, **12**, 8721.

View Article Online
DOI: 10.1039/C6CP01740A

16 J. Jiang, J. K. Zhao, X. Xiao, L. Zhang, *J. Am. Chem. Soc.,* 2012, **134**, 4473.
17 Z. Zhao, Z. Li, Z. Zou, *J. Phys. Condens. Matter*, 2010, **22**, 75008.
18 H. Xu, P. Reunchan, S. Ouyang, H. Tong, N. Umezawa, T. Kako, J. Ye, *Chem. Mater.,* 2013, **25**, 405.
19 J. Yin, Z. Yu, F. Gao, J. Wang, H. Pang, Q. Lu, *Angew. Chem. Int. Ed.,* 2010, **49**, 6328.
20 A. Watt, E. Thomsen, P. Meredith, H. R. Dunlop, *Chem. Commun.,* 2004, 2334.
21 J. Jiang, L. Zhang, H. Li, W. W He, J. J. Yin, *Nanoscale*, 2013, **5**, 10573.
22 R. Yuan, C. Lin, B. Wu, X. Fu, *Eur. J. Inorg. Chem.,* 2009, 3537.
23 H. Peng, C. K. Chan, S. Meister, X. F. Zhang, X. F. Y. Cui, *Chem. Mater.* 2009, **21**, 247.
24 S. K. Poznyak, A. I. Kulak, Electrochim. Acta. 1990, **35**, 1941.
25 J. Henle, P. Simon, A. Frenzel, S. Scholz, S. Kaskel, *Chem. Mater*., 2007, **19**, 366.
26 L. Ye, L. Zan, L. Tian, T. Peng, J. Zhang, *Chem. Commun.,* 2011, **47**, 6951.
27 K. Zhao, L. Zhang, J. Wang, Q. Li, W. He, J. J. Yin, *J. Am. Chem. Soc.* 2013, **135**, 15750.
28 M. Guan, C. Xiao, J. Zhang, S. Fan, R. An, Q. Cheng, J. Xie, M. Zhou, B. Ye, Y. Xie, *J. Am. Chem. Soc.* 2013, **135**, 10411.
29 Y. Wu, B. Yuan, M. Li, W. H. Zhang, Y. Liu, C. Li, *Chem. Sci.*, 2015, **6**, 1873.
30 Y. Myung, F. Wu, S. Banerjee, J. Park, P. Banerjee, *Chem. Commun*., 2015, **51**, 2629.
31 H. Li, L. Zhang, *Nanoscale*, 2014, **6**, 7805.
32 L. Zhang, W. Wang, D. Jiang, E. Gao, S. Sun, *Nanoresearch*, 2014, **3**, 821.
33 X. Liu, H. Yang, H. Dai, X. Mao, Z. A. Liang, *Green Chem. 2015*, **17**, 199.
34 D. G. Shchukin, E. A. Ustinovich, A. I. Kulak, D. V. Sviridov, *Photochem. Photobiol. Sci*., 2004, **3**, 157.
35 M. Law, J. M. Luther, Q. Song, B. k. Hughes, C. L. Perkins, A. J. Nozik, *J. Am. Chem. Soc.* 2008, **130**, 5974.
36 J. Zhang, J. Wang, Z. Zhao, T. Yu, J. Feng, Y. Yuan, Z. Tang, Y. Liu, Z. Li, Z. Zou, *Phys. Chem. Chem. Phys.,* 2012, **14**, 4763.
37 H. Zhang, B. Hu, L. Sun, R. Hovden, F. W. Wise, D. A. Muller, R. D. Robinson, *Nano Lett.*, 2011, **11**, 5356.
38 Y. Lei, G. Wang, S. Song, W. Fan, H. Zhang, *CrystEngComm*, 2009, **11**, 1857.
39 Y. Zhang, X. Xu, Y. Xing, H. Wang, H. Fu, X. Lin, J. Wang, *Adv. Mater. Interfaces*, 2015 DOI: 10.1002/admi.20150019.4
40 Q. Liu, D. Wu, Y. Zhou, H. Su, R. Wang, C. Zhang, S. Yan, M. Xiao, Z. Zou, *ACS Appl. Mater. Interfaces*, 2014, **6**, 2356.
41 X. Zhang, X. B. Wang, L. W. Wang, W. k. Wang, L. L. Long, W. W. Li, H. Q. Yu, *ACS Appl. Mater. Interfaces*, 2014, **6**, 7766.
42 Z. Haider, Y. S. Kang, *ACS Appl. Mater. Interfaces,* 2014, **6**, 10342.
43 J. M. Song, C. J. Mao, H. L. Niu, Y. H. Shen, S. Y. Zhang, *CrystEngComm*, 2010, **12**, 3875.
44 C. Long, H. Fan, *Dalton Trans*., 2012, **41**, 11046.
45 F. Tian, Y. Zhang, G. Li, Y. Liu, R. Chen, *New J. Chem.* 2015, **39**, 1274.
46 K. Zhang, D. Zhang, J. Liu, K. Ren, H. Luo, Y. Peng, G. Li, X. Yu, *CrystEngComm*, 2012, **14**, 700.
47 L. Tang, R. Ji, X. Li, K. S. Teng, S. P. Lau, *J. Mater. Chem. C.,* 2013, **1**, 4908.
48 S. Park, C. W. Lee, M. J. Kang, S. Kim, H. J. Kim, J. E. Kwon, S. Y. Park, C. Y. Kang, K. S. Hong, K. T. Nam, *Phys. Chem. Chem. Phys*., 2014, **16**, 10408.
49 S. Weng, Z. Fang, Z. Wang, Z. Zheng, W. Feng, P. Liu, *ACS Appl. Mater. Interfaces*, 2014, **6**, 18423.
50 F. E Osterloh, *Chem. Soc. Rev.* 2013, **42**, 2294.
51 P. Zhang, X. Li, C. Shao, Y. Liu, *J. Mater. Chem. A*, 2015, **3**, 3281.
52 J. Boltersdorf, N. King, P. A. Maggard, *CrystEngComm.* 2015, **17**, 2225.
53 J. Bisquert, F. F. Santiago, I. M. Sero, G. G. Belmonte, S. Gimenez, *J. Phys. Chem. C*, 2009, **113**, 17278.
54 Z. He, Y. Sheng, Y. Rong, G. D. Lee, J. Li, H. H. Warner, *ACS Nano*, 2015, **9**, 2740.
55 G. Zhang, M. Zhang, X. Ye, X. Qiu, S. Lin, X. Wang, *Adv. Mater.* 2014, **26**, 805.
56 H. Kisch, D. J. Bahnemann, *Phys. Chem. Lett.* 2015, **6**, 1907.
57 W. J. Kim, D. Pradhan, B. k. Min, Y. Sohn, *Appl. Catal. B.* 2014, **147**, 711.
58 Y. Yu, C. Cao, H. Liu, P. Li, F. Wei, Y. Jiang, *J. Mater. Chem. A.* 2014, **2**, 1677.